Assessment of Land and Renewable Energy Resource Potential for Regional Power System Integration with ML Spatio-temporal Clustering

Rosemary E. Alden, Claire Halloran[1], Donovin D. Lewis, Dan M. Ionel, and Malcolm McCulloch[1]

SPARK Laboratory, Stanley and Karen Pigman College of Engineering, University of Kentucky, Lexington, KY, USA
[1]Energy and Power Group (EPG), University of Oxford, Oxford, England

rosemary.alden@uky.edu, claire.halloran@eng.ox.ac.uk, donovin.lewis@uky.edu,
malcolm.mcculloch@eng.ox.ac.uk, dan.ionel@ieee.org

***Abstract*—Toward the planning and development of future electric power systems with extremely large penetration of renewable resources (DERs), detailed assessment of power and energy potential is needed considering both spatial and temporal data per region. Within this paper, a methodology for spatio-temporal DER capacity potential considering land cover types and weather variation are presented using spatio-temporal data. Additionally, an application of empirical orthogonal functions (EOFs) and max-p unsupervised learning techniques is proposed for DER generation to identify zones of similar output power in space and time. A detailed case study for the example region of Kentucky, USA is completed with state-of-the-art utility scale solar photovoltaic (PV) panels, wind turbines, and publicly available data from the National Aeronautics and Space Administration (NASA) Earthdata resource and the National Land Cover Database (NLCD). Annual estimates of wind and solar PV power for the example region are found to meet the state's public annual energy requirement, even in the low land usage case. Further efforts to decarbonize energy generation and build additional renewable energy capacity are supported through the methodology and case study.**

***Index Terms*—Renewable energy, GIS, spatio-temporal modeling, open source modeling, spatial clustering, unsupervised learning**

I. Introduction

As the future of the global electricity infrastructure turns toward renewable distributed energy resources (DERs), advanced modeling of potential generation per region becomes increasingly important. Examples of developed resources for the modeling of DERs include textbooks for MATLAB and ANSYS simulations [1] and open-source tools such as Renewable.ninja [2], Atlite [3], and reV [4] from a universities and national laboratories. Investigations into regional capability to meet local energy requirements with low impact land utilization from renewable generation may aid in the development and adoption of DER technology.

Spatio-temporal clustering may assist modeling of energy systems for cost and operational risk studies. An effort by Scaramuzzino *et al.* in Europe was conducted to assess and cluster land areas based on local weather patterns and identify generation regions by applying k-means classification [5]. Within the reference, the heterogeneity of generation regions including multiple countries was found and a policy recommendation was made for clustered regions to exchange goods and services including renewable energy with each other. Another notable spatio-temporal clustering paper by Jani *et al.* explored regional wind and solar PV power complementarity in India for technical power system and economic projects [6].

Further effort by Fleischer to identify regions of DER generation was shown to reduce the effects of spatial resolution on energy system optimization models (ESOMs) when compared to random regions or existing country boundary lines [7]. In the example case, clustered max-p regions were used to minimize investment and dispatch cost of the power systems across Germany and Spain instead of political regions. Patil *et al.* proposed aggregation techniques for renewable energy and existing power system to reduce complexity and run time of power system energy cost with less than a 5% change in result [8]. Within the U.S.A., climate zones have been identified by ASHRAE standards and used to cluster building stock [9], which parallels the National Renewable Energy Laboratory (NREL) comparison of regional solar PV clusters from different methods that find max-p to be the best performing [10].

A review of ESOM studies by Aryanpur *et al.* compared the results from 22 studies including 36 countries to identify the effects of higher resolution spatial data and when homogeneous regions of renewable energy regions may be used to reduce computation complexity [11]. They found that finer resolution was beneficial in regions with heterogeneity of renewable energy potential, case by case analysis of the relationship between renewables and geography was needed, and that total system costs were under estimated with disaggregation of renewables.

Based on the procedures of the developed DER modeling tools, within this paper, calculations for spatio-temporal wind turbine (WT) and solar photovoltaic (PV) power and annual energy generation considering high resolution land cover are presented for the example region of Kentucky, USA. A general methodology to use benchmark equations for wind and solar PV power and assess the capability for regions to meet energy requirements is described. An application of max-p

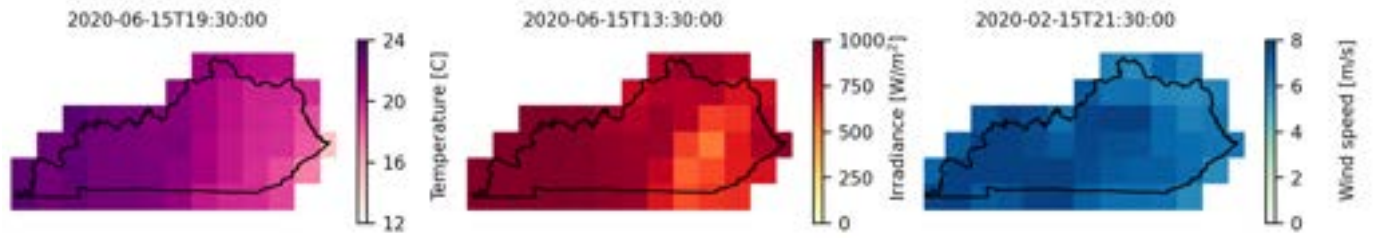

Fig. 1. The temperature, irradiance, and wind speed at 50m for the example land region of Kentucky from the publicly available NASA EarthData Pathfinder. The time of day is selected to show the variation of each weather condition geospatially.

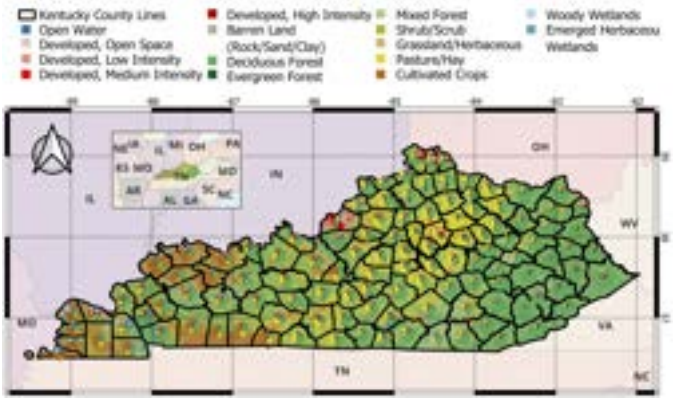

Fig. 2. Land cover data for Kentucky, the region of study, with pie charts generated for each county's composition. Land cover data was considered by category in the estimate of renewable power potential.

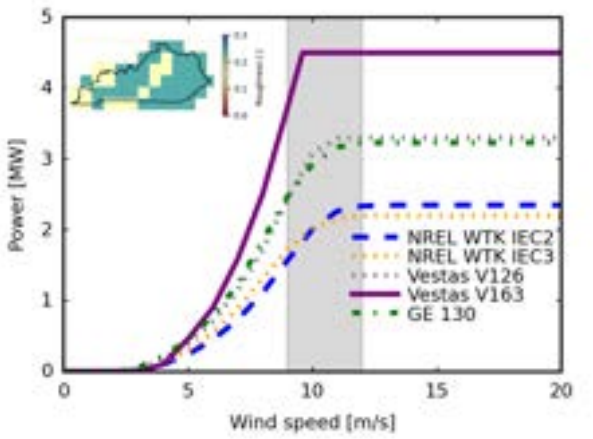

Fig. 3. Publicly available windspeed/power curves for example WTs are depicted from multiple companies and sources. The gray section at the apex of the curves shows for the target wind speeds for high capacity factor output. The 4MW platform Vestas V163 was selected for use in the example study.

regionalization, an unsupervised learning technique, developed and recently published by co-authors Halloran and McCulloch [12], is proposed to cluster for the example region the wind and solar PV generation into zones of similar spatial and temporal variation. The results, which compare favorably with others published in literature based on other methods, may be further employed to maximize renewable generation capacity and minimize required energy storage and land.

II. Geospatial Analysis of DERs

There is great interest in the decarbonization of generation profiles across the world, e.g. [13], and therefore, a major question is whether these regions have the renewable energy potential and site availability for large-scale renewable generation deployment. These calculations provide perspective for the capability of the example region to generate enough renewable energy to self sustain or meet expected annual electrical energy load within the local jurisdiction.

The first public data source employed for wind and solar PV active power calculations was the NASA Earthdata Pathfinder MERRA-2 reanalysis climate data for wind speed at 50m, solar irradiance, and temperature as visualized in Fig. 1 at the hourly and 50km temporal and spatial resolutions [14, 15]. The second public data source, the United States Geological Survey's 2019 release of the National Land Cover Database, was applied for renewable siting exclusion [16]. Within this high resolution satellite imagery data source, land cover classifications were provided for each 30 by 30m of land in the USA including developed land, forest, and cultivated crops. A summary of the land cover data for the example region is depicted in Fig. 2 with a pie chart in each county representing the mixture of land cover types.

Utility scale solar PV and wind turbine generation units were selected for fixed axis commercial installations. Rooftop solar PV, including residential DER generation, was not considered. Example WT power curves for low and medium wind speed from public data sources are illustrated in Fig. 3 [17–19]. The included corner map indicates the roughness coefficients, $\alpha(x, y)$, as defined by matching the land cover type of the maximum area in square (x, y) with the corresponding constant from a comprehensive textbook [20].

The α per each spatial coordinate was applied in hub height scaling of the wind speed, also from [20], across the example region as follows:

$$V_{hub}(t, x, y) = V_0(t, x, y) \left(\frac{H_{hub}}{H_0} \right)^{\alpha}, \qquad (1)$$

where $V_{hub}(t, x, y)$ is the velocity of the wind at the H_{hub} hub height and $V_0(t, x, y)$ is the measurement height. In this

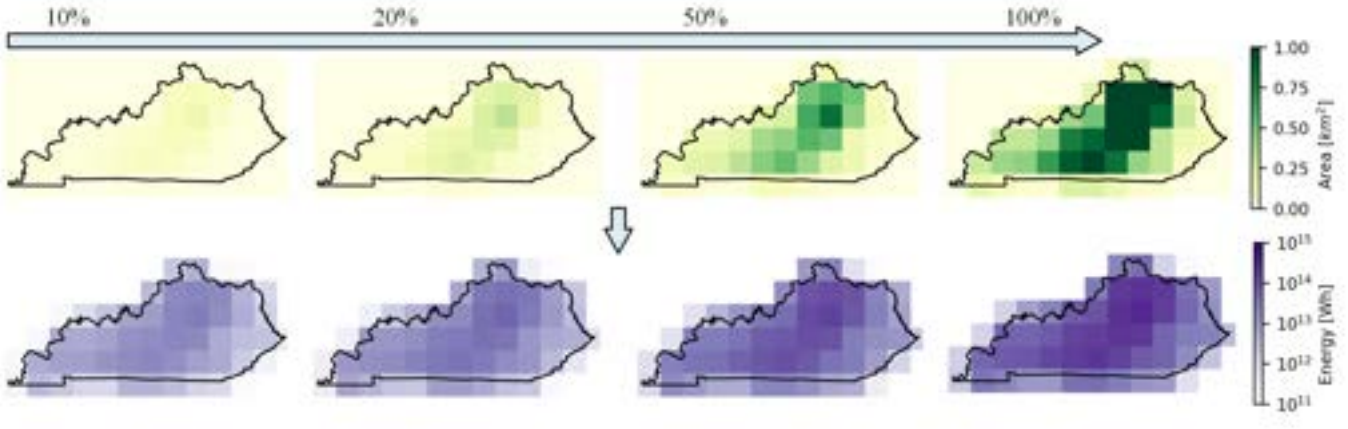

Fig. 4. Designated land area, $a_d(x, y)$, across the example state excludes a buffer of 200m around roads and urban city areas and was scaled in percentage from lower impact to higher impact. The corresponding SunPower SPR-X21-470 example solar PV annual energy in 2020 for each percentage, visualized on a logarithmic scale, suggests a high potential energy region in central KY. Spacing between rows for a 50% packing factor shows the high end of the range of energy provided in Table I.

paper, the V163 turbine on a 4MW platform was selected as an example for high power output at low-medium wind speed in the renewable energy potential estimations with a hub height of 140m.

The specifications for the SunPower SPR-X21-470 solar panel were employed as an example commercial installation from a published data sheet [21]. The AC power for a SunPower single solar PV panel unit, P_{ac}, was calculated according to the benchmark equations in Jones *et al.* [22] and as follows:

$$T_c(t,x,y) = T_{amb}(t,x,y) + \left(\frac{N - 20°C}{0.8}\right)\left(\frac{\gamma(t,x,y)}{1000}\right), \quad (2)$$

$$P_{ac}(t,x,y) = \frac{\gamma(t,x,y)P_r E}{1000}\left(1 - \frac{k_p}{100}[T_c(t,x,y) - h]\right), \quad (3)$$

where t is time; x, y the latitude and longitude coordinates; T_c thecell temperature; γ and T_{amb} the solar irradiance and temperature from the Earthdata MERRA-2 dataset, respectively; N the nominal operating cell temperature of 45°C; P_r is 470W, the rated PV array DC power; E the efficiency of the inverter, interconnection modules, and dirt accumulation; h is 25°C; and k_p is -0.29%/°C for the maximum power temperature coefficient.

With these equations and the WT power curve, renewable power output was estimated for each hour from the single wind and solar PV generation units, P_u $[W/unit]$, in each latitude/longitude square of the 2020 MERRA-2 climate data. To estimate the potential installation capacity and annual energy, the area of the unit itself, a_u and the required additional space was calculated as:

$$a_u = \begin{cases} (a_p + a_r) * d_t, & \text{if } u = \text{Solar PV} \\ (s_x * s_y) * {r_l}^2, & \text{if } u = \text{WT}, \end{cases} \quad (4)$$

where a_p is the panel area (2m^2); a_r the area of space between rows; d_t the ratio of total area of PV facilities to direct area; and $s_{x,y}$ are scalar multipliers for the rotor length, r_l. The d_t of 1.36 and a_r range of 1-3m^2 for packing factors of 50-17% were determined based on a NREL technical report for the land cover of solar PV installations across the USA [23]. The scalar multipliers for s_x and s_y were selected as 5-9 and 3-5 to establish the benchmark range described in [20].

With this unit area, the active renewable power potential given designated land types, P_p, l, across the example region may be calculated as:

$$P_p, l(t,x,y) = \left(\frac{\sum_{n=1}^{N} a_d(x,y)}{a_u}\right) * P_u(t,x,y), \quad (5)$$

where N is the number of designated land types and a_d is the area of the designated land types within the x,y coordinate square. It is important to note that a buffer of 200m from urban areas and primary roads as defined geo-spatially by the United States Homeland Infrastructure Foundation-Level Database [24] was also applied for site exclusion as part of the calculation of $a_d(x, y)$.

III. Case Study of Regional Large-Scale Renewables Integration

The proposed generally applicable method was applied for an example region in the USA state of Kentucky in two detailed case studies with varied designated land types and DER generation unit spacing corresponding to lower and higher land usage. Land cover types applicable for the example region were selected depending on the generation unit, either PV panel or WT, from the total area of classified land types. Barren land, shrub/scrub, and pasture/hay were selected for solar PV due to their low height land occupancy and the potential for dual-usage including livestock grazing, native pollination, etc. Within the solar PV case study, percentages of the designated land areas from 10-100% were applied to provide estimates with low and high impact on land utilization in the state (Fig. 4).

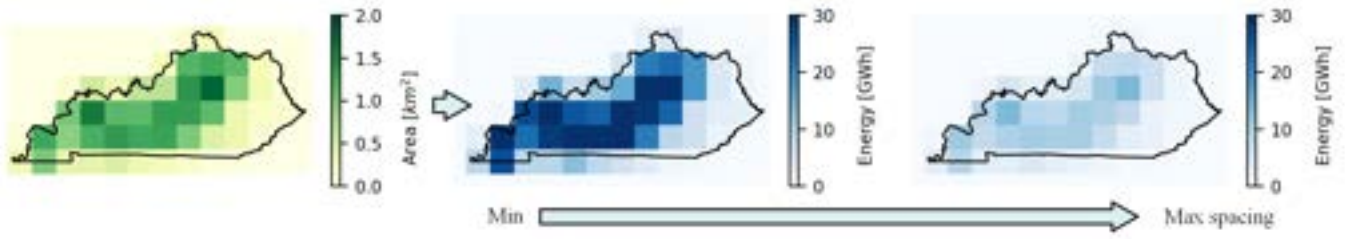

Fig. 5. As the land area in WT facilities is multi-use, the entire area of the designated land coverage types was employed in this case study. The corresponding annual energy output for the example V163 with minimum and maximum spacing shows high generation regions excluding forests.

Table I
RESULTS OF KENTUCKY REGIONAL CASE STUDY: ANNUAL ELECTRICAL ENERGY FOR KY REACHED ABOVE 89 TWH

Renewable Type	Designated Area [km^2]	Kentucky Land [%]	Maximum Count [gen. unit]	Power Capacity [TW]	Annual Energy [TWh]
Solar (100% a_d)	2.2 x 10^4	21	3.2 – 5.6 x 10^9	1.5 – 2.6	2300 – 4000
Solar (10% a_d)	2.2 x 10^3	2.1	3.2 – 5.6 x 10^8	0.15 – 0.26	230 – 400
Solar (100% a_d^*)[1]	1.1 x 10^3	1	1.6 – 2.8 x 10^8	0.08 – 0.13	110 – 200
Wind	3.3 x 10^4	31	2.8 – 8.2 x 10^4	0.124 – 0.369	0.251 – 0.748

[1]Additional case with the designated area for solar PV, a_d^*, of barren and shrub land only.

Wind turbine designated area was expanded to included cultivated crops, as the low ground area utilization and high operation height of WT technology allow for further use of underlying land. Designated land cover types selected for wind generation were also intentionally conservative, not including typical sites such as forests or altitude which can greatly alter overall performance and may be some of the best places to install. As land occupied by WTs technology is commonly considered multi-use, percentage cases were not conducted, and the conservative designated land estimate with areas of high annual generation are visualized in Fig. 5.

For wind generation, the potential power and annual energy output are orders of magnitude smaller than for solar PV generation, despite the fact that the designated area is 50% larger. The difference in example V163 wind and SPR-X21-470 solar PV potential may partially be explained by the overall packing factor or capability to fill a designated land area with generation units. The size per MW for the chosen WT and solar PV panel ranges from maximum to minimum fill of 22.2 – 66.3 acres/MW and 1.9 – 3.1 acres/MW. These estimates are both within the size range summaries for wind and solar PV technology reported by NREL of 44.7$\pm$25 and 3.2$\pm$2.2 acres/MW, respectively [25].

Results for the Kentucky case study are listed in Table I, including the designated land area, maximum generation unit count considering minimum and maximum spacing, power capacity, and annual energy per renewable type. Total wind and solar PV designated land coverage separately account for approximately 21% and 31% of the total 104,656km^2 Kentucky land area, respectively. Ranges are shown for the number of generation units, power capacity, and annual energy as the minimum and maximum spacing for solar PV and WTs were considered.

Assuming an annual electrical energy of 89TWh in the target region [26], the percentage of land area dedicated to solar PV generation was varied such that the total energy generated would be equivalent. Within this case study, it was found that energy equal to the annual electrical energy assumed may be generated using 2% of the designated solar PV area including pasture and hay, which is 0.5% of total land in the region. The power capacity using 2% of designated solar PV area is 58GW, approximately six times the expected peak load.

If the full 21% of designated land area was used for solar PV units, annual energy upto 4,000TWh may be generated, more than the 2020 USA energy of 3,800TWh [27] and 45 times the annual Kentucky electrical energy. An additional case study for solar PV was performed to exclude pasture land, which has deep cultural significance in the region. It was estimated that the annual energy of 89TWh [26] may be met using 45% of barren and shrub land, i.e. 0.5% of total state area, with a 50% packing factor.

IV. WIND AND SOLAR PV OUTPUT ZONES

The method for spatial-temporal clustering, previously developed and recently published by co-authors Halloran and McCulloch [12], is briefly reviewed in the following, applied to a regional study in Kentucky, and results favorably compared with those published for the example region by other research groups using different methods. The method is based on Empirical Orthogonal Function (EOF) analysis and max-p regionalization, which has been used in climate studies to identify spatial patterns in weather variability by calculating the eigenvalues and eigenvectors of a spatially weighted anomaly covariance matrix of a field [28], in this case hourly wind and solar PV potential at each location. In preparation for max-p region clustering, EOF analysis was used for dimensionality reduction.

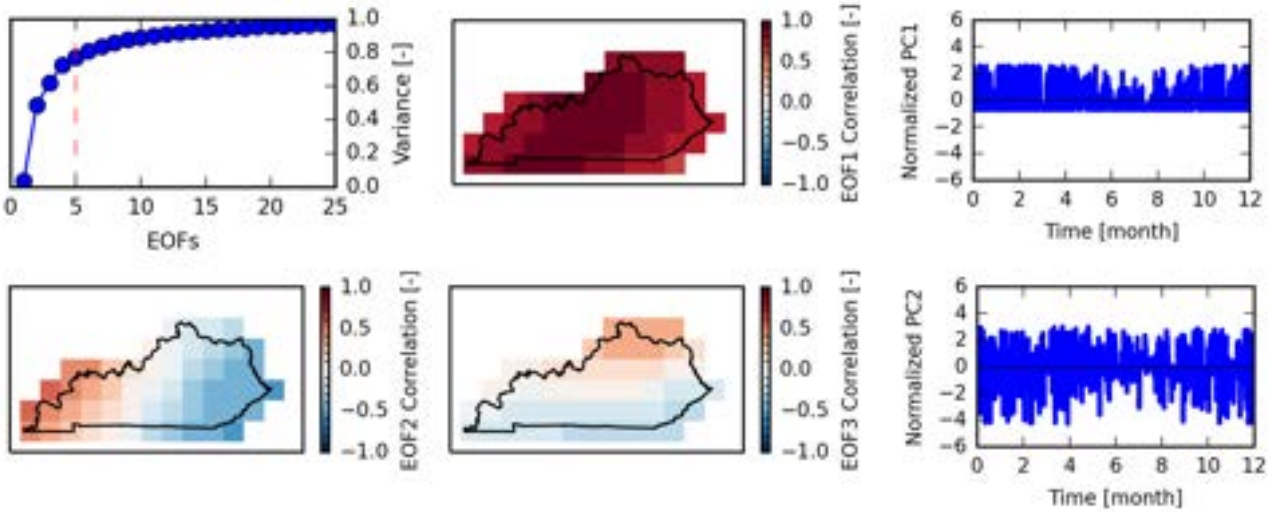

Fig. 6. The EOF anaylsis was applied to the spatio-temporal Vestas V163 wind power, P_u [W/unit], in the example region for the year 2020. The first five EOFs account for 95% of the variance in the 3D input matrix. The first principal component (PC) capturing seasonal influence, followed by geographical factors in the remaining EOFS and PCs.

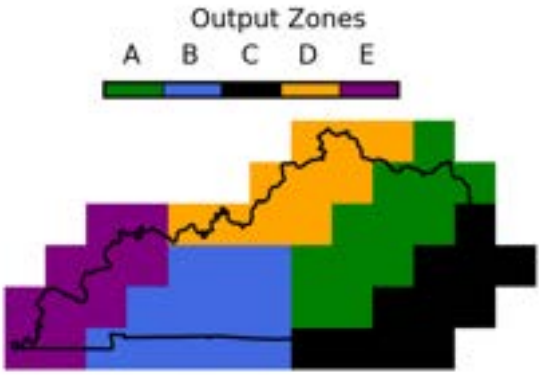

Fig. 7. Example wind power output zones from max-p regionalization for the target area with a minimum zonal threshold of 30,000m^2 align with geological features, such as along mountain lines.

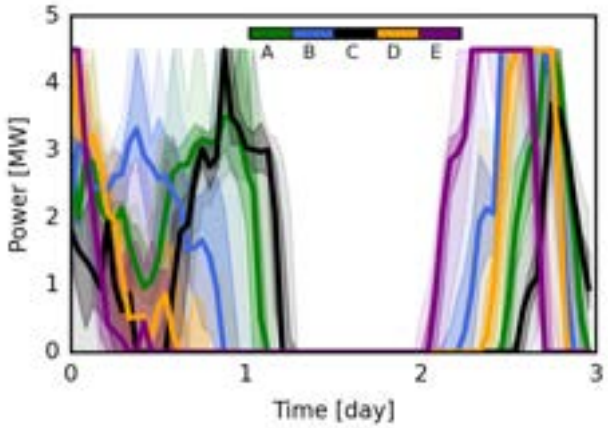

Fig. 8. Time-series wind power for each of the example clusters with darker transparent shading added for the middle 50% and lighter shading for the enter range of the clustered 50km x, y squares. Stopping and starting of wind power intentionally selected to show distinctive behavior between zones.

Each spatial mode corresponds to a principal component (PC) time series and an EOF, a spatial map of correlation with that principal component. The first few PCs and EOFs typically explain a large share of the variance as shown in Fig. 6 for solar generation. The "eofs" python library [29] was employed to perform EOF analysis on hourly wind and solar generation, P_u [W/unit], in the year of 2020. Example EOF and PC results for the target region are visualized in Fig. 6 for wind power with the seasonal variation (EOF1) and spatial location East to West (EOF2) then North to South (EOF3) accounting for the highest shares of variance.

The unsupervised machine learning technique of max-p regionalization was employed to cluster the first five EOFs for wind and solar PV power, P_u [W/unit], into zones following the heuristic proposed by Wei *et al.* [30] in the "spopt" python library [31, 32]. The identified max-p regions for wind P_u [W/unit] with a threshold area of 30,000m^2 are illustrated in Fig. 7. Distinctive profiles for each output zone are show in Fig. 8 with the three days intentionally selected for visualization of power generation variance between zones.

V. Discussion and Scalability

The combination of spatio-temporal renewable energy estimation and clustering for an example region enables many opportunities for decarbonization planning. The utilization of open-source satellite data for renewable energy potential estimation may enable informed decision-making for potential developers without high-resolution locally measured data. Considering constraints such as land coverage and, in future work, transmission-level interconnection may inform both the amount of land and investment needed for suitable energy generation to meet regional load. Example studies with renewable integration into the electric grid system include [33, 34].

With the introduction of further renewables, there comes a point when additional demand is not met by increased generation without the integration of energy storage or zero-carbon firm generation. For the target region, which is served by multiple utilities [35], example dispatches with solely renewable energy are illustrated in Fig. 9(a) and (b) for a

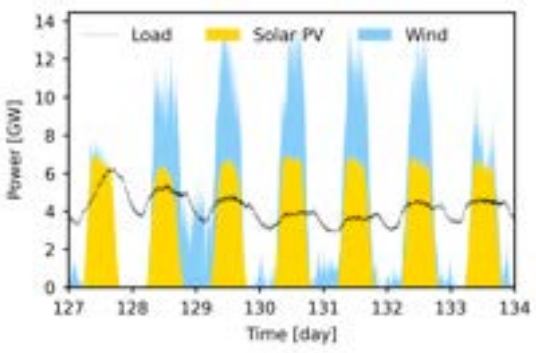

(a)

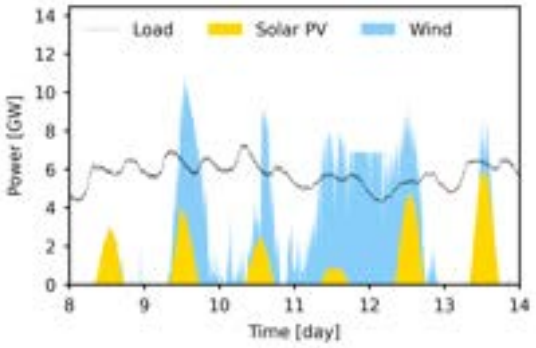

(b)

Fig. 9. Example synthetic renewable energy generation and load for the target region in a summer week (a) and a winter week (b) indicates that increased renewable penetration does not solely meet greater unfulfilled demand without energy storage.

summer and winter week, respectively. Across the synthetic day in the summer and winter, large imbalances arise from the temporal mismatch between weather-varying generation and demand, requiring diurnal storage such as batteries. The significant reduction in renewable output in the winter, Fig. 9(b), compared to summer, Fig. 9(a) necessitates seasonal storage such as green hydrogen.

Spatio-temporal clustering of renewable energy potential could aid both in the siting and sizing of renewable generation capacity and the planning/deployment of diurnal and seasonal storage, such as green hydrogen optimal placement in [36]. Identifying regions with similar renewable potential may allow for extrapolation of limited high-resolution monitoring across a large region, which is additionally beneficial in areas with lower data availability. Effective spatial clustering of temporal power output could reduce the number of machine learning forecasting models required to estimate future generation with less data. Optimal siting of renewable generation across clusters could exploit generation diversity to minimize energy storage requirements. Additionally, cluster level or homogeneous potential may be compared with the state-wide potential to find target development areas when including substation limitations like those depicted in Fig. 10 for the target region.

VI. Conclusion

The spatio-temporal unsupervised machine learning method proposed in the paper is based on EOF and max-p regionalization for the identification of large continuous land zones of similar DER power generation. The generally applicable analysis has been demonstrated for a regional case study in Kentucky, USA, using solely publicly available data for weather and land coverage. Additional computational studies indicate that solar PV and wind have large generation potential, such that that only a very low percentage of the total land may be required to meet the example region's annual electrical energy. This result is comparable with other published studies that employed different methods.

Fig. 10. Transmission lines and substations according to the US HIFLD [24] are located in high density in the areas of renewable potential, specifically in central and northern parts. Further considerations of line and substation ratings, capacity, and location are needed to support studies for a future smart grid with 100% DER generation.

Time analysis exemplified the possible large differences for instantaneous electric power between load and renewable generation and may support adequate sizing of short and long-term energy storage solutions, including electrochemical batteries and green hydrogen. The zonal analysis is also advantageous in identifying optimal placement for representative advanced experimental weather stations and location coordination with transmission substations for electric interconnection. Large-scale computationally efficient power system may use the zonal regions for the integration of diverse generation sources.

Acknowledgment

The material is based upon work supported by the National Aeronautics and Space Administration (NASA) and the Kentucky Space Grant Consortium under the NASA award number 80NSSC20M0047. The support of the National Science Foundation (NSF) GRF grant No. 1839289 and of the Rhodes Trust is also gratefully acknowledged. Any findings and conclusions expressed herein are those of the authors and do not necessarily reflect the views of the sponsor organizations.

References

[1] F. Blaabjerg and D. M. Ionel, *Renewable energy devices and systems with simulations in MATLAB® and ANSYS®*. Boca Raton, FL: CRC Press, 2017.

[2] S. Pfenninger and I. Staffell, "Long-term patterns of European PV output using 30 years of validated hourly reanalysis and satellite data," *Energy*, vol. 114, pp. 1251–1265, 2016. [Online]. Available: https://www.sciencedirect.com/science/article/pii/S0360544216311744

[3] F. Hofmann, J. Hampp, F. Neumann, T. Brown, and J. Hörsch, "atlite: A Lightweight Python Package for Calculating Renewable Power Potentials and Time Series," Jun. 2021.

[4] G. Mclaurin, N. Grue, A. Lopez, D. Heimiller, M. Rossol, G. Buster, and T. Williams, "The renewable energy potential (reV) model:a geospatial platform for technical potential and

supply curve modeling," National Renewable Energy Laboratory (NREL), Tech. Rep. TP-6A20-73067, 2021.
[5] C. Scaramuzzino, G. Garegnani, and P. Zambelli, "Integrated approach for the identification of spatial patterns related to renewable energy potential in European territories," *Renewable and Sustainable Energy Reviews*, vol. 101, pp. 1–13, 2019. [Online]. Available: https://www.sciencedirect.com/science/article/pii/S1364032118307275
[6] H. K. Jani, S. S. Kachhwaha, G. Nagababu, and A. Das, "Temporal and spatial simultaneity assessment of wind-solar energy resources in India by statistical analysis and machine learning clustering approach," *Energy*, vol. 248, p. 123586, 2022. [Online]. Available: https://www.sciencedirect.com/science/article/pii/S0360544222004893
[7] C. E. Fleischer, "Minimising the effects of spatial scale reduction on power system models," *Energy Strategy Reviews*, vol. 32, p. 100563, 2020. [Online]. Available: https://www.sciencedirect.com/science/article/pii/S2211467X20301164
[8] S. Patil, L. Kotzur, and D. Stolten, "Advanced spatial and technological aggregation scheme for energy system models," *Energies*, vol. 15, no. 24, 2022. [Online]. Available: https://www.mdpi.com/1996-1073/15/24/9517
[9] H. Bergmann, H. H. III, and H. Rozenfeld, "Building stock sementation cluster development," U.S. Department of Energy. office of Energy Efficiency & Renewable Energy, Tech. Rep. DOE/GO-102023-5835, 2023.
[10] D. Getman, A. Lopez, T. Mai, and M. Dyson, "Methodology for clustering high-resolution spatiotemporal solar resource data," National Renewable Energy Laboratory (NREL), Tech. Rep. TP-6A20-63148, 2015.
[11] V. Aryanpur, B. O'Gallachoir, H. Dai, W. Chen, and J. Glynn, "A review of spatial resolution and regionalisation in national-scale energy systems optimisation models," *Energy Strategy Reviews*, vol. 37, p. 100702, 2021. [Online]. Available: https://www.sciencedirect.com/science/article/pii/S2211467X21000882
[12] C. Halloran and M. McCulloch, "Spatial clustering of temporal energy profiles with empirical orthogonal functions and max-p regionalization," *ArXiv*, August 2023. [Online]. Available: https://doi.org/10.48550/arXiv.2308.12274
[13] D. D. Lewis, A. Patrick, E. S. Jones, R. E. Alden, A. A. Hadi, M. D. McCulloch, and D. M. Ionel, "Decarbonization analysis for thermal generation and regionally integrated large-scale renewables based on minutely optimal dispatch with a Kentucky case study," *Energies*, vol. 16, no. 4, 2023. [Online]. Available: https://www.mdpi.com/1996-1073/16/4/1999
[14] Global Modeling and Assimilation Office (GMAO) , "MERRA-2 tavg1_2d_rad_nx: 2d, 1-Hourly, Time-Averaged,Single-Level, Assimilation, Radiation Diagnostics V5.12.4," Greenbelt, MD. USA. [Online]. Available: https://disc.gsfc.nasa.gov/datasets/M2T1NXRAD_5.12.4/summary
[15] Global Modeling and Assimilation Office (GMAO), "MERRA-2 tavg1_2d_slv_nx: 2d, 1-Hourly, Time-Averaged, Single-Level,Assimilation, Single-Level Diagnostics V5.12.4," Greenbelt, MD, USA. [Online]. Available: https://disc.gsfc.nasa.gov/datasets/M2T1NXSLV_5.12.4/summary
[16] J. Dewitz, "National Land Cover Database (NLCD) 2019 Products," 2021. [Online]. Available: https://www.sciencebase.gov/catalog/item/5f21cef582cef313ed940043
[17] L. Bauer and M. Silvio, "Wind turbines database," publisher: Deutsche Windtechnik. [Online]. Available: https://en.wind-turbine-models.com/turbines
[18] I. Staffell, "Wind turbine power curves," publisher: Imperial College London, UK. [Online]. Available: https://www.academia.edu/1489838/Wind_Turbine_Power_Curves
[19] "4 MW Platform | Vestas." [Online]. Available: https://www.vestas.com/en/products/4-mw-platform
[20] M. M. Gilbert, "Renewable and efficient electric power systems," Hoboken, NJ, 2004.
[21] "SunPower X-Series Commercial Solar Panels | X21-470-COM Datasheet," Jun. 2020. [Online]. Available: https://us.sunpower.com/sites/default/files/sunpower-x-series-commercial-solar-panels-x21-470-com-datasheet-524935-revb.pdf
[22] E. S. Jones, R. E. Alden, H. Gong, A. G. Frye, D. Colliver, and D. M. Ionel, "The effect of high efficiency building technologies and PV generation on the energy profiles for typical US residences," in *ICRERA*, 2020, pp. 471–476.
[23] S. Ong, C. Campbell, P. Denholm, R. Margolis, and G. Heath, "Land-use requirements for solar power plants in the United States," National Renewable Energy Laboratory (NREL), Tech. Rep. TP-6A20-56290, 2013.
[24] "HIFLD Open Data," accessed October 2022. [Online]. Available: https://hifld-geoplatform.opendata.arcgis.com/
[25] "Land Use by System Technology," publisher: U.S. Department of Energy. [Online]. Available: https://www.nrel.gov/analysis/tech-size.html
[26] "State of Kentucky | Energy Sector Risk Portfolio," Sep. 2016. [Online]. Available: https://www.energy.gov/sites/prod/files/2016/09/f33/KY_Energy%20Sector%20Risk%20Profile.pdf
[27] "SAS Output." [Online]. Available: https://www.eia.gov/electricity/annual/html/epa_02_02.html
[28] "The climate data guide: Empirical orthogonal function (EOF) analysis and rotated eof analysis." [Online]. Available: https://climatedataguide.ucar.edu/climate-data-tools-and-analysis/empirical-orthogonal-function-eof-analysis-and-rotated-eof-analysis
[29] A. Dawson, "eofs: A Library for EOF Analysis of Meteorological, Oceanographic, and Climate Data," *Journal of Open Research Software*, vol. 4, no. 1, p. 14, Apr. 2016. [Online]. Available: https://openresearchsoftware.metajnl.com/article/10.5334/jors.122/
[30] R. Wei, S. Rey, and E. Knaap, "Efficient regionalization for spatially explicit neighborhood delineation," *International Journal of Geographical Information Science*, vol. 35, no. 1, pp. 135–151, Jan. 2021. [Online]. Available: https://www.tandfonline.com/doi/full/10.1080/13658816.2020.1759806
[31] X. Feng, J. D. Gaboardi, E. Knaap, S. J. Rey, and R. Wei, "pysal/spopt," Jan 2021. [Online]. Available: https://github.com/pysal/spopt
[32] X. Feng, G. Barcelos, J. D. Gaboardi, E. Knaap, R. Wei, L. J. Wolf, Q. Zhao, and S. J. Rey, "spopt: a python package for solving spatial optimization problems in pysal," *Journal of Open Source Software*, vol. 7, no. 74, p. 3330, 2022. [Online]. Available: https://doi.org/10.21105/joss.03330
[33] B. Azibek, N. Zhakiyev, A. Ibraimova, and Y. Akhmetbekov, "Increasing total hosting capacity using energy storages during renewable energy expansion," in *ICRERA*, 2022, pp. 414–417.
[34] K. E. Ouedraogo, P. Oğuz Ekim, and E. Demirok, "Decimal states smart grid operations concept: Technical solution and benefit for renewable energy integration," in *ICRERA*, 2022, pp. 174–178.
[35] E. Moser, "Kentucky energy profile. 8th edition," Kentucky Energy and Environment Cabinet (EEC), Tech. Rep., 2023. [Online]. Available: https://eec.ky.gov/Energy/KY%20Energy%20Profile/Kentucky%20Energy%20Profile%202023.pdf
[36] L. A. Müller, A. Leonard, P. A. Trotter, and S. Hirmer, "Green hydrogen production and use in low- and middle-income countries: A least-cost geospatial modelling approach applied to Kenya," *Applied Energy*, vol. 343, p. 121219, 2023. [Online]. Available: https://www.sciencedirect.com/science/article/pii/S0306261923005834